NUMERICAL SOLUTION OF THE NAVIER-STOKES EQUATIONS

FOR ARBITRARY TWO-DIMENSIONAL MULTI-ELEMENT AIRFOILS*

Joe F. Thompson, Louie Turner, W. Serrill Long, and John H. Bearden
Mississippi State University

SUMMARY

The development of a numerical simulation of time-dependent, turbulent, compressible flow about two-dimensional multi-element airfoils of arbitrary shape is described. The basis of this simulation is a technique of automatic numerical generation of coordinate systems fitted to the multiple bodies regardless of their number or shape.

Incompressible solutions have been run for NACA airfoils at Reynolds numbers as high as 10^6, but present drag predictions are about twice the experimental values. Procedures have been developed whereby the coordinate lines are automatically concentrated in the boundary layer at any Reynolds number. The compressible turbulent solution involves an algebraic eddy viscosity turbulence model. The laminar version has been run for transonic flow at free-stream Mach numbers up to 0.9.

INTRODUCTION

The overall purpose of the present research project is to develop a numerical simulation of time-dependent, turbulent, compressible flow about two-dimensional multi-element airfoils of arbitrary shape. The basis of this simulation is a technique of automatic numerical generation of coordinate systems fitted to the multiple bodies regardless of their number or shape. This procedure eliminates the shape of the bodies as a complicating factor and allows the flow about arbitrary bodies to be treated essentially as easily as that about simple bodies. All computation can be done on a rectangular transformed field with a square mesh regardless of the shape or number of bodies in the physical field.

In the effort thus far, numerical solutions have been developed for the time-dependent incompressible Navier-Stokes equations for laminar flow about arbitrary multiple airfoils, and the compressible Navier-Stokes equations for laminar and turbulent flow about single airfoils. Continuous refinement of the techniques is being made as higher Reynolds numbers are considered. A number of papers have reported the work so far in references 1-8, and the coordinate system code has been made available for general use as described in reference 8.

C-3

The development of the compressible turbulent solution is now being extended to multiple airfoils using a new coordinate system configuration having the infinity boundary collapsed to a point. Refinement of this solution and the incompressible solution for multiple airfoils is also continuing. Finally, the search for improvements in the iterative solutions involved continues in order to improve the computational efficiency of all the solutions.

Symbols are defined in an appendix.

BOUNDARY-FITTED COORDINATE SYSTEM

General Formulation

The basic idea of the boundary-fitted coordinate systems is to numerically generate a curvilinear coordinate system having some coordinate line coincident with each boundary of the physical region of interest, regardless of the shape of these boundaries. This is done by taking the curvilinear coordinates to be solutions of an elliptic partial differential system, with constant values of one of the curvilinear coordinates specified as Dirichlet boundary conditions on each boundary. Values of the other coordinate are either specified in a monotonic variation over a boundary as Dirichlet boundary conditions, or are determined by Neumann boundary conditions thereon. In the latter case, the curvilinear coordinate lines can be made to intersect the boundary according to some specified condition, such as normalcy or parallel to some given direction. It is also possible to exercise control over the spacing of the curvilinear coordinate lines in the field in order to concentrate lines in regions of expected high gradients.

In any case, the numerical generation of the coordinate system is done automatically for any shape boundaries, requiring only the input of points on the boundary. The technique has been described in detail in earlier reports (ref. 1 and 7) and the computer code, together with instructions for and examples of its use in the numerical solution of partial differential equations, is given in reference 8.

As mentioned previously, the curvilinear coordinates are generated by solving an elliptic system of suitable form. One such system is

$$\xi_{xx} + \xi_{yy} = P(\xi, \eta) \tag{1a}$$

$$\eta_{xx} + \eta_{yy} = Q(\xi, \eta) \tag{1b}$$

with Dirichlet boundary conditions, one coordinate being specified to be equal to a constant on the body and equal to another constant on the outer boundary, with the other coordinate varying monotonically over the same range around both the body and the outer boundary.

184

Since it is desired to perform all numerical computations in the uniform rectangular transformed plane, the dependent and independent variables must be interchanged in Eq. (1). This results in the coupled system

$$\alpha x_{\xi\xi} - 2\beta x_{\xi\eta} + \gamma x_{\eta\eta}$$

$$= - J^2 [x_\xi P(\xi,\eta) + x_\eta Q(\xi,\eta)] \tag{2a}$$

$$\alpha y_{\xi\xi} - 2\beta y_{\xi\eta} + \gamma y_{\eta\eta}$$

$$= - J^2 [y_\xi P(\xi,\eta) + y_\eta Q(\xi,\eta)] \tag{2b}$$

where

$$\alpha = x_\eta^2 + y_\eta^2 \qquad\qquad \gamma = x_\xi^2 + y_\xi^2$$

$$\beta = x_\xi x_\eta + y_\xi y_\eta \qquad\qquad J = x_\xi y_\eta - x_\eta y_\xi$$

(Transformation relations are given in ref. 8).

The system described by eq. (2) is a quasilinear elliptic system for the coordinate functions $x(\xi,\eta)$ and $y(\xi,\eta)$ in the transformed plane. This set is considerably more complex than the linear system specified by eq. (1), but the boundary conditions are specified on straight boundaries, and the coordinate spacing in the transformed plane is uniform.

The coordinate lines may be spaced as desired around the boundaries, since the assignment of the coordinate values to the [x,y] boundary points is arbitrary. Control of the radial spacing of the coordinate lines is accomplished by varying the functions $P(\xi,\eta)$ and $Q(\xi,\eta)$ in equations (2).

Automatic Concentration of Coordinate Lines into a Boundary Layer

Consider the coordinate system generation equations (2) applied to the one-dimensional case of straight boundaries parallel to the x-axis. With η = constant on these boundaries, and the ξ-lines being normal to the boundaries, we have $y_\xi = y_{\xi\xi} = y_{\xi\eta} = 0$, and the x-equation is identically zero so

that the coordinate equations reduce to

$$\gamma y_{\eta\eta} + J^2 Q y_\eta = 0 \qquad (3)$$

This can be made a perfect differential by choosing the form of the control function Q to be

$$Q(\eta) \equiv -\frac{\gamma}{J^2} \frac{f''(\eta)}{f'(\eta)} \qquad (4)$$

where the minus sign has been introduced merely for convenience. Then eq. (3) can be integrated to yield

$$y(\eta) = c_1 f(\eta) + c_2 \qquad (5)$$

The constants of integration may be evaluated from the boundary conditions: $y(1) = y_1$, $y(J) = y_J$ so that

$$y(\eta) = y_1 + (y_J - y_1) \left(\frac{f(\eta) - f(1)}{f(J) - f(1)} \right) \qquad (6)$$

This equation can then be solved for $f(\eta)$ to yield

$$\frac{f(\eta) - f(1)}{f(J) - f(1)} = \frac{y(\eta) - y_1}{y_J - y_1} \qquad (7)$$

which, with arbitrary definition of $f(1)$ and $f(J)$, will yield the required $f(\eta)$, and hence the required $Q(\eta)$ via substitution in eq. (4), to produce a desired distribution $y(\eta)$. The evaluation of $Q(\eta)$ may be done without actual evaluation of $f(\eta)$, however, by solving eq. (3) for Q to produce

$$Q(\eta) = -\frac{\gamma}{J^2} \frac{y''}{y'} \qquad (8)$$

Now a number of smooth functions for $y(\eta)$, such as exponentials, logarithmic functions, hyperbolic functions, etc., may be found which will concentrate lines near y_1 with a spread out to y_2. However, since the boundary

layer thickness at high Reynolds number is only a very small fraction of the distance to outer boundary of the computational field, such smooth functions cannot allow the lines to spread rapidly enough outside of the boundary layer. The result is that nearly all of the lines in the field will be within a few boundary layer thicknesses of the body, with a great gap near the outer boundary.

Therefore, a composite function was used for $y(\eta)$, formed by joining a logarithmic function to a quartic polynomial near the edge of the boundary layer. This function is constructed as follows: assume that it is desired to space the lines in the boundary layer such that the change in velocity from each to the next is the same. Let the velocity profile in the boundary layer be approximated by the exponential

$$u(y) = 1 - e^{-cy} \tag{9}$$

Let the edge of the boundary layer be defined by

$$u = 0.99 \text{ at } y = \delta$$

Then the decay factor c will be given by

$$c = -\frac{1}{\delta} \ln (0.01)$$

Now solve eq.(9) for $y(u)$:

$$y(u) = -\frac{1}{c} \ln (1-u) \tag{10}$$

In order to achieve the same velocity change from each line to the next, take $u = 0.99 \, (\frac{n-1}{n_\delta - 1})$ where n_δ is the line at the edge of the boundary layer. Substitution in eq. (10) then yields

$$y(\eta) = -\frac{1}{c} \ln [1 - 0.99 \, (\frac{n-1}{n_\delta - 1})], 1 \le \eta \le \eta_\delta \tag{11}$$

Let this logarithmic function be joined to a quartic polynomial at some line inside or at the outer edge of the boundary layer. Thus with the function at $\eta = N$, the polynomial is of the form

$$y(\eta) = y'(N) \ [\eta - N] + \frac{1}{2} \ y''(N) \ [\eta - N]^2$$

$$+ \frac{1}{6} \ y''(N) \ [\eta - N]^3 + a(\eta - N)^4 + y(N)$$

$$N \le \eta \le J \tag{12}$$

Here $y'(N)$ is functional notation, etc. The derivatives are determined by differentiation of eq. (11), with evaluation at $\eta = N$. The remaining coefficient "a" is used to satisfy the boundary condition at the outer boundary, $y(J) = y_J$. Thus

$$a = \frac{y_J - y(N) - y'(N) \ [J-N] - \frac{1}{2} y''(N) \ [J-N]^2 - \frac{1}{6} y''(N) [J-N]^3}{(J-N)^4}$$

Note that the junction to the polynomial need not occur at the edge of the boundary layer, but anywhere inside it. It has been found advantageous to place the junction two or three lines inside the boundary layer.

Thus if the boundary layer thickness, δ, and the number of lines therein, η_δ, are specified, along with the distance to the outer boundary, y_J, and the total number of lines J, and the junction line N, the control function $Q(\eta)$ can be evaluated from

$$Q(\eta) = -\frac{\gamma}{J^2} \ \frac{\frac{0.99}{\eta_\delta - 1}}{1 - 0.99 \ (\frac{\eta-1}{\eta_\delta - 1})}, \eta = 1, 2, --, \ N \le \eta_\delta \tag{13a}$$

$$Q(\eta) = -\frac{\gamma}{J^2} \ \frac{y'(N) + y''(N) \ [\eta-N] + 12a[\eta-N]^2}{y'(N) + y''(N) \ [\eta-N] + \frac{1}{2} y''(N) \ [\eta-N]^2 + 4a[\eta-N]^3}$$

$$\eta = N, \ N+1, \ ---, \ J \tag{13b}$$

with the required derivatives given by

$$y^{(k)}(N) = \frac{\frac{(k-1)!}{c} \ (\frac{0.99}{N-1})^k}{[1 - 0.99 \ (\frac{\eta-1}{N-1})]^k}, \ k = 1, 2, 3 \tag{14}$$

188

and y(N) by

$$y(N) = -\frac{1}{c} \ln[1 - 0.99 \, (\frac{N-1}{n_\delta - 1})]$$ (15)

Although this analysis is developed for the one-dimensional case of a flat boundary, the same general results will be achieved by its use with curved boundaries since curvature tends to affect both the boundary layer thickness and the line control in the same way. Thus convex curvature thins the boundary layer but also causes the lines to concentrate to a greater degree near the boundary.

An example of coordinate systems generated with this concentration of lines in boundary layers is shown in figure 1.

The exponential velocity distribution in eq. (9) may be replaced by the Blasius distribution, and this has been done in practice since a more even spacing is obtained in the lower part of the boundary layer in that case.

Truncation Error Induced by the Coordinate System

Some attention must be paid to the rapidity of the change of coordinate line spacing with strong attraction, else truncation error in the form of artificial diffusion may be introduced as follows: Consider the finite difference approximation of a first derivative with variation only in the x-direction to which the ξ-lines are normal. Then

$$f_x = \frac{y_\eta f_\xi}{x_\xi y_\eta} = \frac{f_\xi}{x_\xi}$$ (16)

The difference approximation then would be

$$f_x = \frac{f_{i+1} - f_{i-1}}{x_{i+1} - x_{i-1}} + T_i$$ (17)

where T_i is the local truncation error. Taylor series expansions of f_{i+1} and f_{i-1} about f_i then yield, after some algebraic rearrangement,

$$T_i = -\frac{1}{2} (f_{xx})_i \, (x_{i+1} + x_{i-1} - 2x_i)$$ (18)

189

But the last factor is simply the difference approximation of $x_{\xi\xi}$ so that

$$T = \frac{1}{2} x_{\xi\xi} f_{xx}$$

This truncation error thus introduces a numerical diffusive effect in the difference approximation of first derivatives. Care must therefore be taken that the second derivatives of the physical coordinates (i.e., the rate of change of the physical spacing between curvilinear coordinate lines) are not too large in regions where the dependent variables have significant second derivatives in the direction normal to the closely spaced coordinate lines.

Just what is a permissible upper limit to the rate of change of the line spacing is problem dependent. Consider, for instance, viscous flow past an infinite flat plate parallel to the x-direction. Here the velocity parallel to the wall changes rapidly from zero at the wall to its free stream value over a small distance that is of the order of $\frac{1}{\sqrt{R}}$, where R is the Reynolds number, $R = \frac{U_\infty x}{\nu}$, based on freestream velocity, U_∞, the distance from the leading edge of the plate, x, and the kinematic viscosity, ν. The equation for the time rate of change of the velocity parallel to the wall is

$$u_t = -uu_x - vu_y + \frac{1}{R}(u_{xx} + u_{yy}) \tag{19}$$

Recalling that the large spacial variation in velocity occurs in the y-direction, coordinate lines would be contracted near the plate. The truncation error introduced by this contraction would be

$$T(v) = \left(-\frac{v}{2} y_{\eta\eta}\right) u_{yy} \tag{20}$$

This introduces a negative numerical viscosity $\left(-\frac{v}{2} y_{\eta\eta}\right)$, since v and $y_{\eta\eta}$ are both positive.

The effective viscosity is thus reduced (effective Reynolds number increased), so that the velocity gradient near the wall is steepened. Therefore care should be taken that $y_{\eta\eta}$ is limited so that the numerical viscosity $\left(-\frac{v}{2} y_{\eta\eta}\right)$ is not significant in comparison with the physical term $\left(\frac{1}{R}\right)$. The situation is mitigated somewhat of the fact that the numerical viscosity is proportional to the small velocity normal to the wall, this velocity being of order $\frac{1}{\sqrt{R}}$. Actually this limit is conservative, since the normal velocity drops to zero at the wall and only attains the order $\frac{1}{\sqrt{R}}$ on the outer portion

of the region of large gradient of velocity parallel to the wall, where u_{yy} is very small.

Transformation of Infinity to an Interior Circuit

With multiple-bodies involving two closely-spaced bodies, the coordinate line spacing in the area between the bodies will not be too good with the type of coordinate system generated by the original TOMCAT code (ref. 8) as illustrated in figure 2. This results from the smoothness of solutions of Poisson equations, the contours of which tend to avoid concave regions. Coordinate system control can improve the situation somewhat as shown in reference 3.

However, with two bodies, an even better system can be obtained by first transforming the remote outer boundary circle to a small interior circle, or even a point, by the analytical complex transformation $Z' = \frac{1}{Z}$. Here $Z = x + iy$ is a point in the physical plane, while $Z' = x' + iy'$ is a corresponding point in the transformed plane. These original and transformed boundary circuits are illustrated in figs. 3&4 for an airfoil-flap combination.

The coordinates (x', y') of the transformed boundary circuits are then input to the TOMCAT code in the usual manner, with the body circuits comprising the entire top and bottom sides of the rectangular transformed plane and one half of the small outer boundary circle appearing on a portion of the left and right sides. The result of the TOMCAT code, in the form of ξ and η lines drawn in the $x' - y'$ plane, is shown in fig. 5 for a wing-slat.

The inverse analytic transformation, $Z = \frac{1}{Z'}$, back to the $x - y$ plane then produces coordinate lines of constant ξ and η in the $x - y$ plane as shown in figs. 6-8, the second figure being an expanded view of the slot region. A similar coordinate system for a leading edge slat configuration is shown in figs. 9&10.

INCOMPRESSIBLE SOLUTION

The incompressible solution is written in the primitive variable formulation, and some description has been given in reference 3. The solution is completely implicit, so that all equations are solved simultaneously at each time step. The construction essentially parallels that described for the compressible solution in the next section, with the exception that the Poisson equation for the pressure has no time derivative, of course. On the airfoil surface, the pressure is determined by iteratively adjusting the pressure at each point on the surface in proportion to the divergence of the velocity at the same point, so that upon convergence the continuity equation is satisfied on the airfoil surface (ref. 3).

This code has been written with great generality, so that it can serve as a research tool with which different numerical representations can be evaluated. The following features can be selected simply by input options without changing the code:

(a) 2-point central convective derivatives
(b) 6-point central convective derivatives
(c) 2-point upwind convective derivatives
(d) 3-point upwind convective derivatives
(e) 4-point cross derivatives
(f) 7-point cross derivatives
(g) product-of-average nonlinear terms
(h) average-of-product nonlinear terms
(i) fully nonlinear
(j) second-order linearization
(k) conservative form
(l) nonconservative form
(m) time-dependent form
(n) steady-state form

Input options can also select several starting procedures as follows:

(a) Impulsive start from rest
(b) Impulsive start from potential flow
(c) Accelerating start from rest
(d) Decreasing penetration start
(e) Increasing Reynolds number start

The pressure boundary condition can be selected as from the continuity equation as discussed above or from the normal momentum equation applied on the body. These boundary conditions can be either first or second order. The time derivative can be either first or second order, and first or second-order projection can be used for the initial guess for the iteration at each time step if desired. Diffusion based on the change between time steps can be activated if desired, as can be flux-corrected transport or a two cell wave length filter.

The code also contains the following choices of iteration scheme, with selection by input option:

(a) point SOR with computed acceleration parameters
(b) line SOR, either rows or columns
(c) ADI
(d) Stone strongly implicit

The point SOR iteration uses a variable acceleration parameter field, the parameter at each point being continually adjusted to be equal to the locally linearized optimum. This feature is important at high Reynolds number since the optimum acceleration parameter depends on both the local velocity and the mesh spacing. Finally, a multi-grid iteration form of this same code has been written, and three variations of the multi-grid algorithm are now under study.

These codes treat the full incompressible Navier-Stokes equations for any number of multiple bodies and thus can handle all configurations produced by the TOMCAT coordinate code. Experimentation is now in progress with all these options at high Reynolds number.

The incompressible Navier-Stokes solution has also been written in the vorticity-stream function formulation (ref. 6) and in the integro-differential (vorticity-velocity) formulation (ref. 9), as well as the primitive variable formulation discussed above. Results for flow about NACA single symmetric and 6-series airfoils at high Reynolds number (10^6) have been obtained. These high Reynolds number results, however, predict drag that is about twice the experimental value, indicating the need for further development.

Some typical results as described in ref. 9 are shown in figures 11-13 for a Reynolds number of 10^6. Some lower Reynolds number results for a multiple airfoil are shown in figs. 14-16.

COMPRESSIBLE SOLUTION

Numerical Formulation

The compressible solution is based on the full Navier-Stokes equations in fully conservative form in the transformed coordinates. At the interior field points, a second-order backward time, central space scheme is used to represent the differential equations. Along the body surface, the continuity equation is represented using second-order, one-sided space differences.

Turbulence Model

The compressible code also includes an algebraic two-layer turbulent eddy viscosity model as used in reference 10 (termed Model 3 therein).

Results

The compressible code is still under development, but preliminary results are shown in figs. 17-21 for a NACA 0018 airfoil at 5° angle of attack, Mach number of 0.9, Reynolds number of 20,000, and surface temperature of 0.8.

The Mach contours in figure 18 show a rather diffuse shock and the thick boundary layer resulting from the somewhat low Reynolds number. The velocity vectors of figure 19 indicate separation on the upper surface. The peak in the density profiles ahead of and behind the airfoil (fig. 21) are compression and expansion waves resulting from the impulsive start from incompressible potential flow.

CONCLUDING REMARKS

Both the incompressible and compressible solutions are still under development. The search also continues for the most appropriate multi-element coordinate configurations. As noted, a wide variety of numerical procedures is under evaluation in order to develop an efficient treatment of high Reynolds number flow.

APPENDIX

SYMBOLS

ξ	Curvilinear Coordinate
η	Curvilinear Coordinate
x	Cartesian Coordinate
y	Cartesian Coordinate
P	Coordinate Control Function for ξ
Q	Coordinate Control Function for η
α	Metric Function Defined with Equations (2)
β	Metric Function Defined with Equations (2)
γ	Metric Function Defined with Equations (2)
J	Jacobian, Also Total Number of Coordinate Lines Around Body
f	General Function
c_1, c_2	Constants of Integration
c	Exponential Decay Factor
u	Velocity Component
δ	Boundary Layer Thickness
M	Free-stream Mach Number
N	Junction Line
a	Coefficient in Quartic Polynomial
T	Truncation Error
t	Time
R	Reynolds Number
v	Velocity Component
z	Complex Variable

194

Subscripts

ξ Denotes Differentiation with Respect to ξ

η Denotes Differentiation with Respect to η

x Denotes Differentiation with Respect to x

y Denotes Differentiation with Respect to y

t Denotes Differentiation with Respect to t

δ Denotes Value at Edge of Boundary Layer

J Denotes Value at Outer Boundary

N Denotes Value at Junction Line

REFERENCES

1. Thompson, J. F., Thames, F. C., and Mastin, C. W., "Automatic Numerical Generation of Body-Fitted Curvilinear Coordinate System for Fields Containing Any Number of Arbitrary Two-Dimensional Bodies," Journal of Computational Physics, 15, 299, (1974).

2. Thames, F. C., Thompson, J. F., and Mastin, C. W., "Numerical Solution of the Navier-Stokes Equations for Arbitrary Two-Dimensional Airfoils," Proceedings of NASA Conference on Aerodynamic Analyses Requiring Advanced Computers, Langley Research Center, NASA SP-347, (1975).

3. Thompson, J. F., Thames, F. C., Mastin, C. W., and Shanks, S. P., "Use of Numerically Generated Body-Fitted Coordinate Systems for Solution of the Navier-Stokes Equations," Proceedings of the AIAA 2nd Computational Fluid Dynamics Conference, Hartford, Connecticut, (1975).

4. Thompson, J. F., Thames, F. C., Shanks, S. P., Reddy, R. N., and Mastin, C. W., "Solutions of the Navier-Stokes Equations in Various Flow Regimes on Fields Containing Any Number of Arbitrary Bodies Using Boundary-Fitted Coordinate Systems," Proceedings of V International Conference on Numerical Methods in Fluid Dynamics, Enschede, the Netherlands, Lecture Notes in Physics, Springer-Verlag, (1976), Vol. 59, p. 421.

5. Thompson, J. F., Warsi, Z. U. A., and Amlicke, B. B., "Numerical Solutions for Laminar and Turbulent Viscous Flow Over Single and Multi-Element Airfoils Using Body-Fitted Coordinate Systems," Advances in Engineering Science, Proceedings of 13th Annual Meeting Society of Engineering Science Hampton, Virginia, (1976), NASA CP-2001.

6. Thames, F. C., Thompson, J. F., Mastin, C. W., and Walker, R. L., "Numerical Solutions for Viscous and Potential Flow About Arbitrary Two-Dimensional Bodies Using Body-Fitted Coordinate Systems," Journal of Computational Physics, 24, 245 (1977).

7. Thompson, J. F., Thames, F. C., Mastin, C. W., "TOMCAT - A Code for Numerical Generation of Boundary-Fitted Curvilinear Coordinate Systems on Fields Containing Any Number of Arbitrary Two-Dimensional Bodies," Journal of Computational Physics, 24, 274 (1977).

8. Thompson, J. F., Thames, F. C., and Mastin, C. W., "Boundary-Fitted Curvilinear Coordinate System for Solution of Partial Differential Equations on Fields Containing Any Number of Arbitrary Two-Dimensional Bodies," NASA CR-2729 (1977).

9. Reddy, R. N. and Thompson, J. F., "Numerical Solution of Incompressible Navier-Stokes Equations in the Integro-Differential Formulation Using Boundary-Fitted Coordinate Systems," Proceedings of the AIAA 3rd Computational Dynamics Conference, Albuquerque, 1977.

10. Deiwert, G. S., "Computational of Separated Transonic Turbulent Flows," AIAA Journal, 14, 735 (1976).
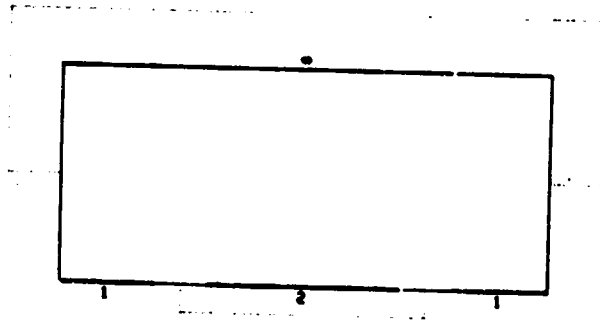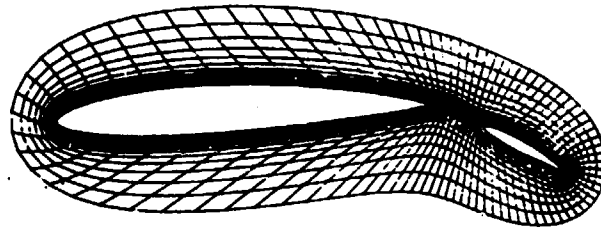
Figure 1.- Wing-flap coordinate system. Original COMCAT form.
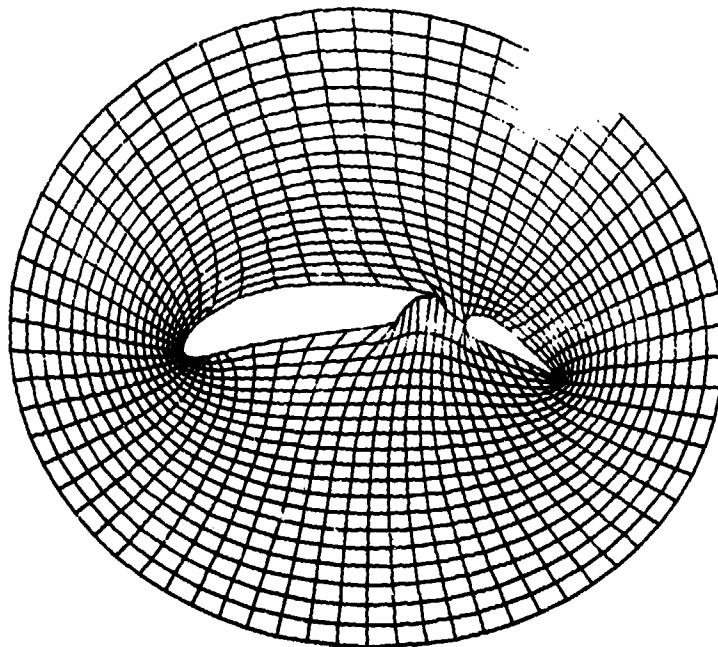
Figure 2.- Wing-flap coordinate system. Poor spacing in concave region.

197
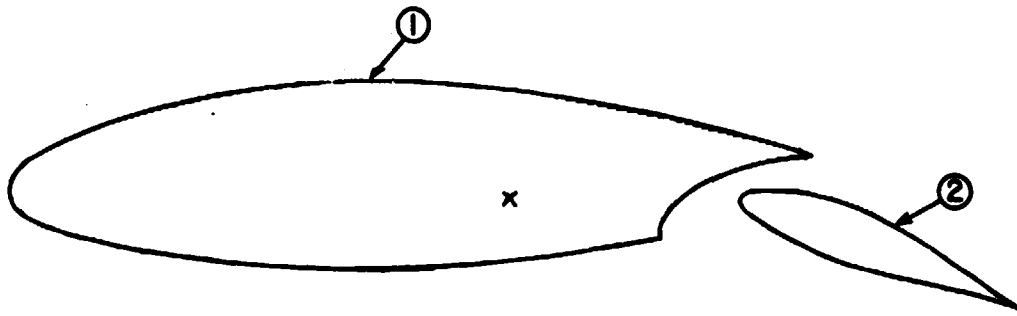
Figure 3.- Modified NACA 64_3-418 wing flap.
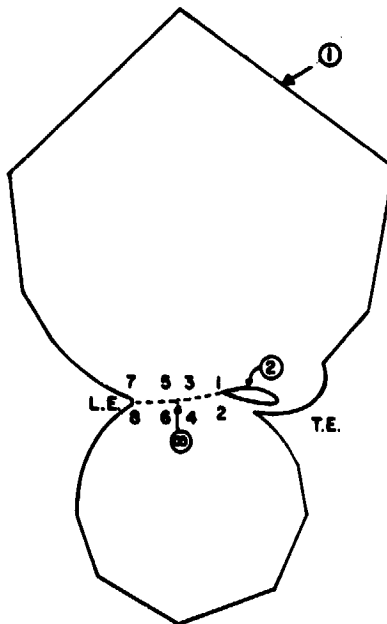
Figure 4.- Transformed modified wing-flap configuration.
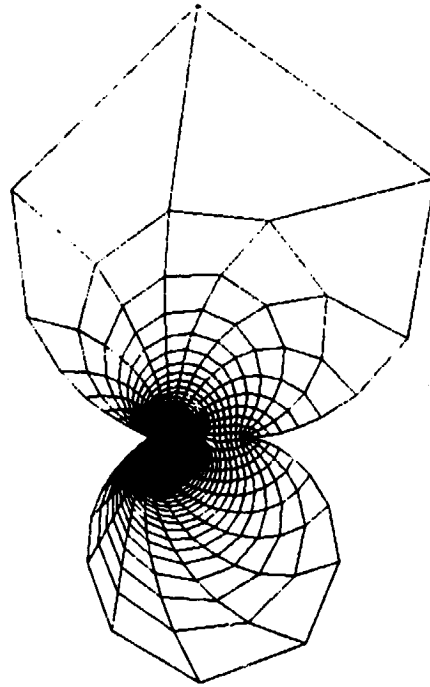
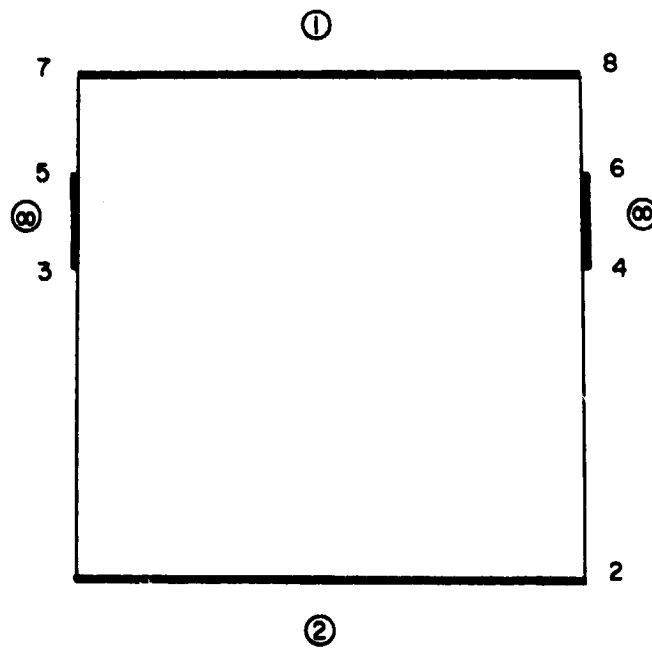Figure 5.- Coordinate lines in transformed plane for wing slat.

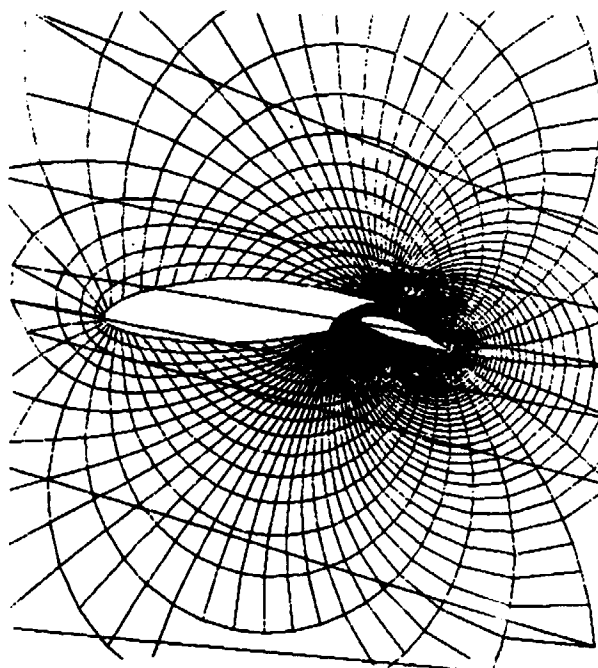Figure 6.- Rectangular computational plane for wing flap.
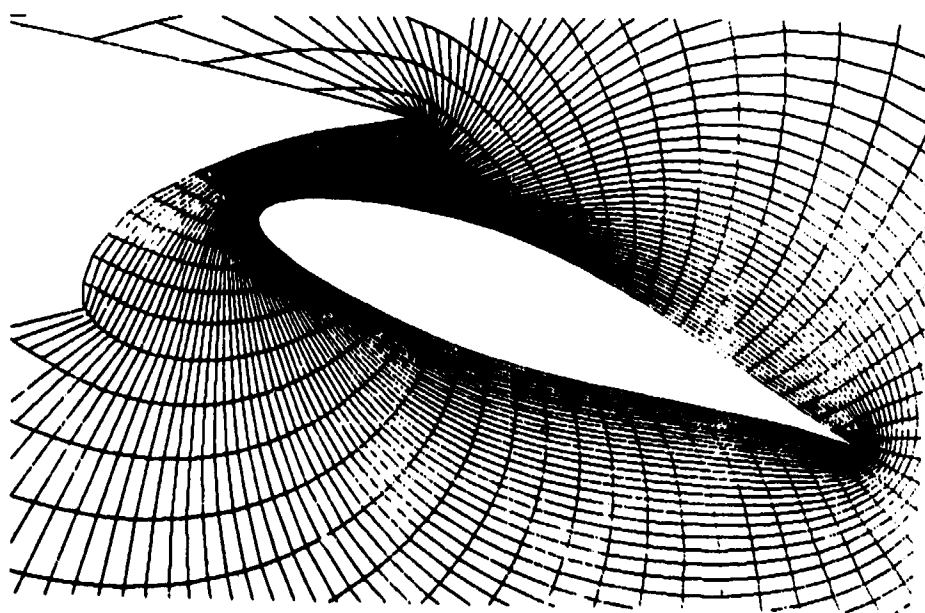
Figure 7.- Wing-flap coordinate system.
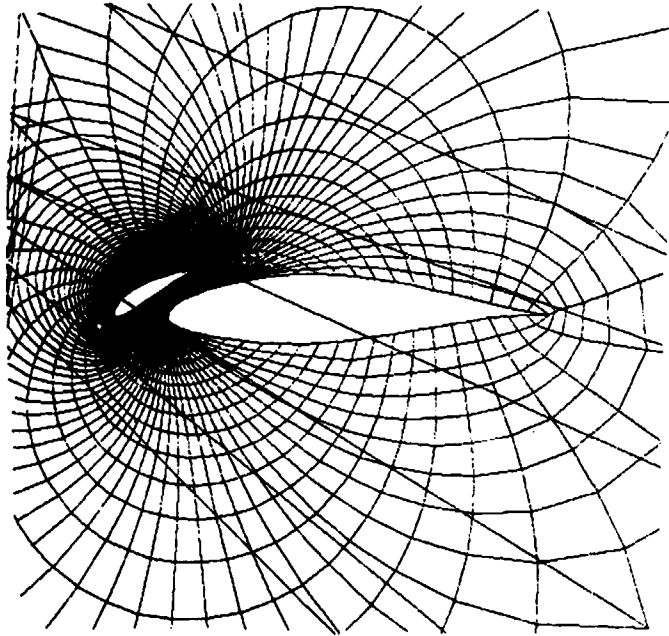

Figure 8.- Expanded view of wing-flap coordinate system.

200

Figure 9.- Wing-slat coordinate system.
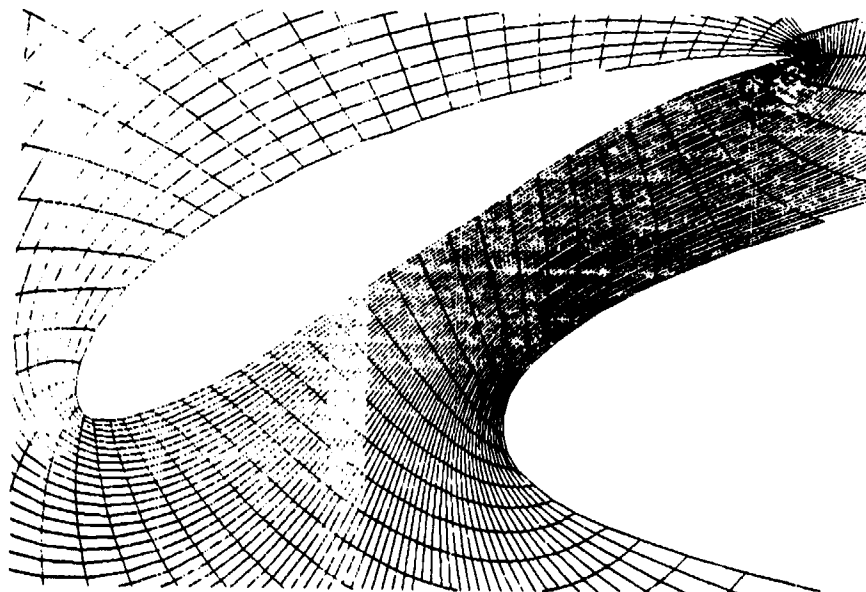
Figure 10.- Expanded view of wing-slat coordinate system.
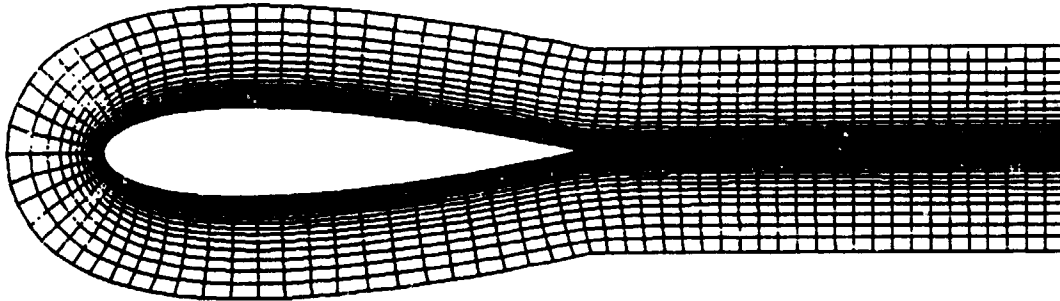
Figure 11.- Coordinate system of NACA 0018 airfoil.   R = 1,000,000.
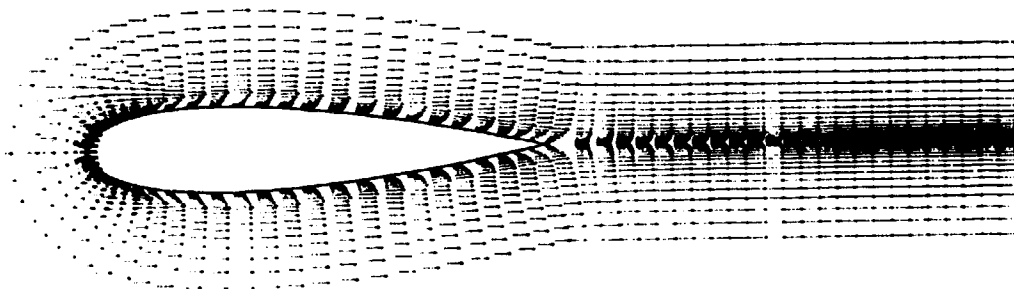
Figure 12.- Velocity vector field of NACA 0018 airfoil.   R = 1,000,000;
$\theta = 0^{\circ}$; T = 2.25.

202
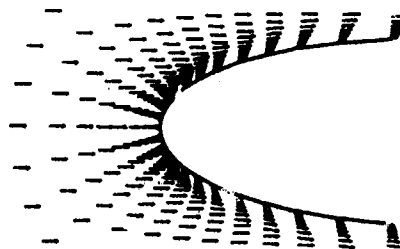
LEADING EDGE DETAILS
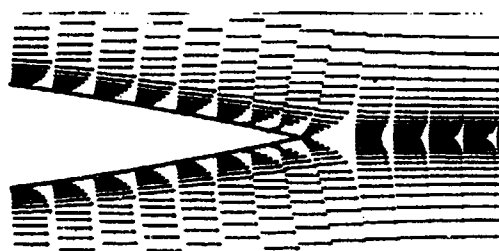
TRAILING EDGE DETAILS

Figure 13.- Velocity vector field of NACA 0018 airfoil. Leading- and trailing-edge details; R = 1,000,000; θ = 0°; T = 2.25.
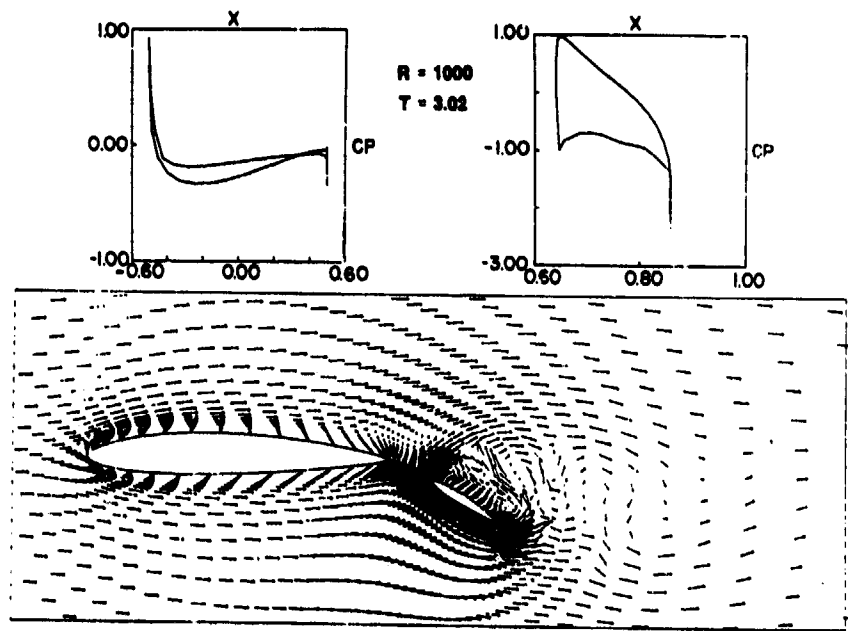
Figure 14.- Multiple airfoil.
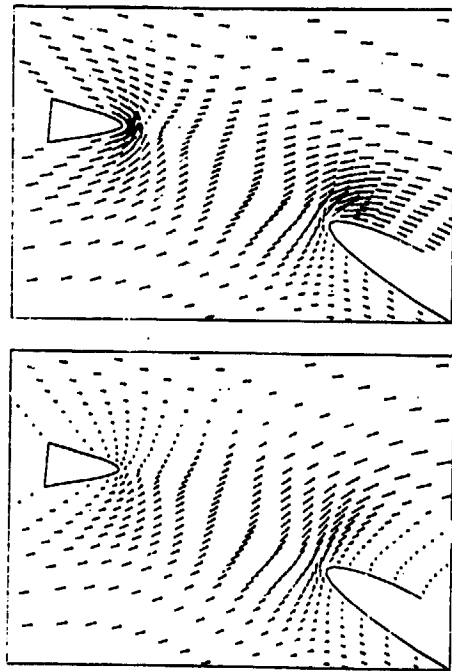
R = 1000, T = 0.01 and 1.2

Figure 15.- Slot detail of multiple airfoil.
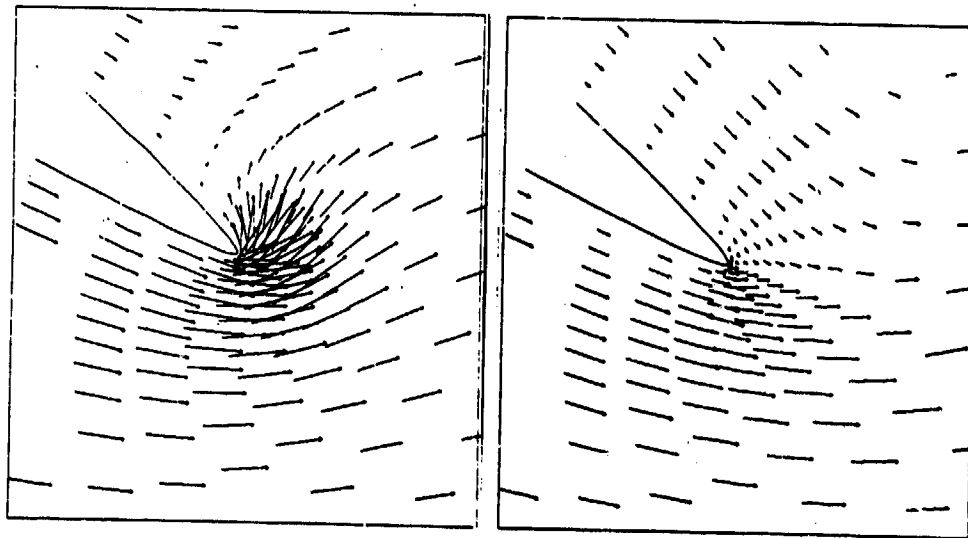
R = 1000, T = 0.01 and 3.02

Figure 16.- Aft trailing-edge detail of multiple airfoil.
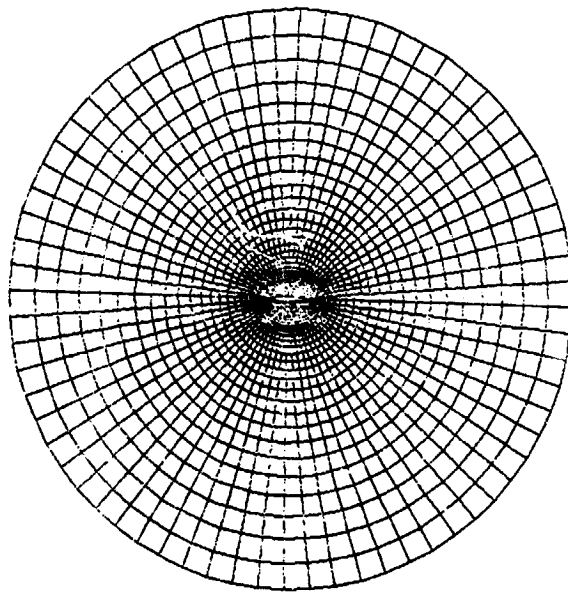
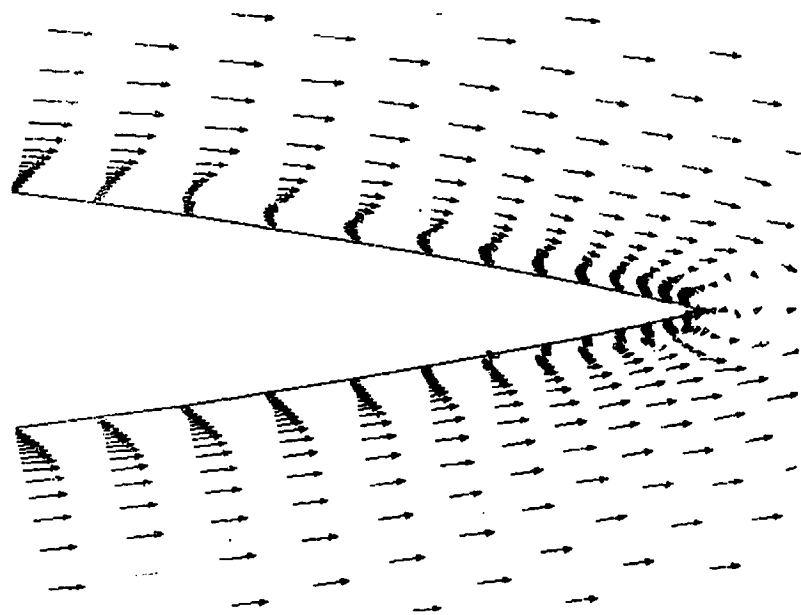Figure 17.- Coordinate system of NACA 0018 airfoil.   R = 20,000.
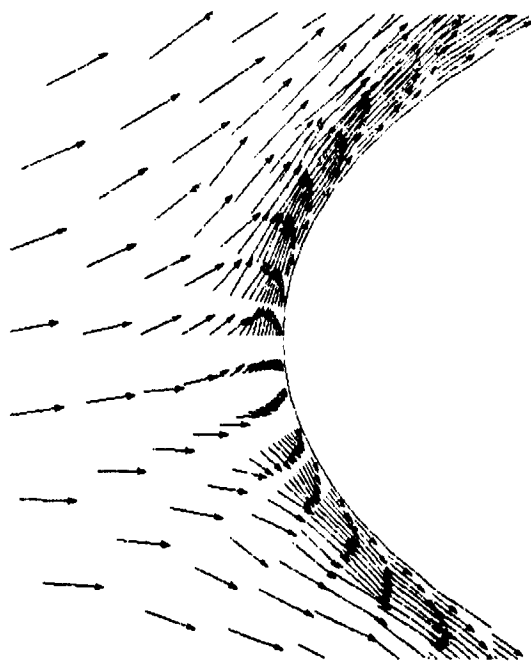
CONTOUR INTERVAL: 0.05
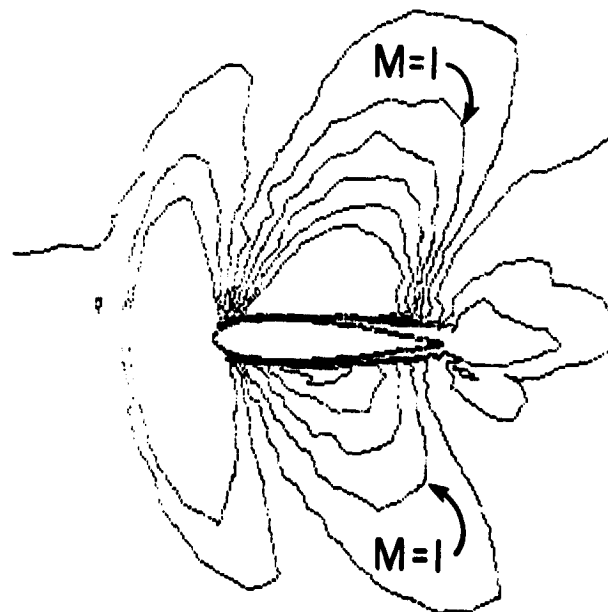
Figure 18.- Mach contours. M_∞ = 0.9: R = 20,000; θ = 5°; T = 1.277.

(a) Trailing edge.

(b) Leading edge.

Figure 19.- Velocity vectors. $M_\infty = 0.9$; $R = 20,000$; $\theta = 5^{\circ}$; $T = 1.277$.
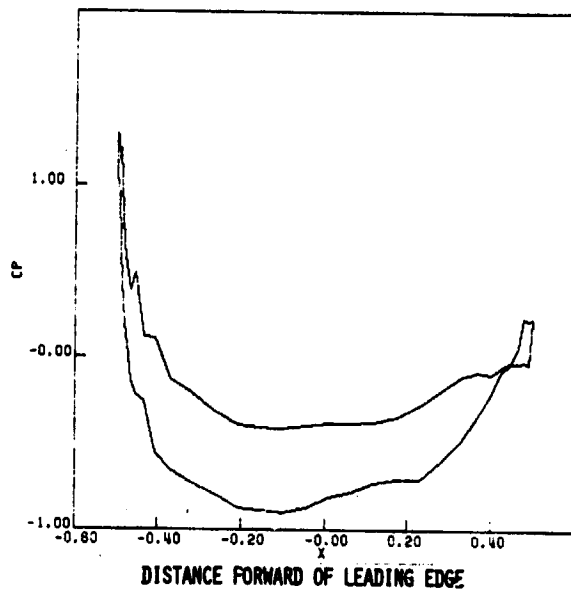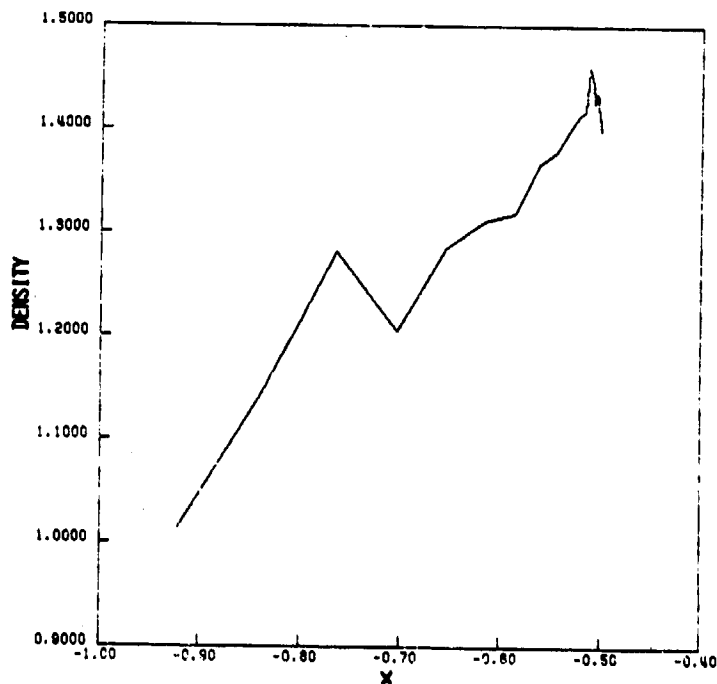
Figure 20.- Surface pressure.

Figure 21.- Density forward of leading edge.